



Identification of Urban Climate Risk Zones Using GIS and Remote Sensing Technology: A Comparative Analysis of Dhaka and Rajshahi City Corporation, Bangladesh



Tasneem Sharmin[✉], Mahinoor Islam Tonmoy^{*}, Morium Ahmed[✉]

Department of Geography & Environment, University of Dhaka, 1000 Dhaka, Bangladesh

* Correspondence: Mahinoor Islam Tonmoy (mahinoorislam-65-2019016137@geoenv.du.ac.bd)

Received: 05-09-2025

Revised: 06-26-2025

Accepted: 07-10-2025

Citation: T. Sharmin, M. I. Tonmoy, and M. Ahmed, "Identification of urban climate risk zones using gis and remote sensing technology: A comparative analysis of Dhaka and Rajshahi City Corporation, Bangladesh," *J. Urban Dev. Manag.*, vol. 4, no. 3, pp. 171–189, 2025. <https://doi.org/10.56578/judm040301>.



© 2025 by the author(s). Licensee Acadlore Publishing Services Limited, Hong Kong. This article can be downloaded for free, and reused and quoted with a citation of the original published version, under the CC BY 4.0 license.

Abstract: Rapid urbanization in Bangladesh has exponentially exacerbated environmental stressors, most notably in Dhaka and Rajshahi, where climate-related concerns are becoming more prevalent. This study adopted geographic information system (GIS) and remote sensing techniques to delineate and assess climate risk zones in Dhaka City Corporation (DCC) and Rajshahi City Corporation (RCC) in 2020 and 2024. The evaluation involved the incorporation of land use/land cover (LULC), land surface temperature (LST), and air pollution indicators. Sentinel-2A multispectral imager (MSI) was used to calculate LULC, Landsat-8 optical land imager (OLI) for LST, and Sentinel-5P for atmospheric pollutants, such as NO₂, SO₂, CO, and PM_{2.5}. The analysis revealed that the built-up land in Dhaka was expanded by 4.38% whereas in Rajshahi, it was 8.91%. Rajshahi recorded a maximum LST of 46.7°C in 2024, when compared to 37.6°C in Dhaka. The level of air pollution was consistently high in Dhaka, with an average concentration of NO₂ reaching 36.4 μmol/m², almost quadrupled the 9.81 μmol/m² in Rajshahi. Weighted overlay analysis demonstrated that 5.38% and 1.63% of the areas in Dhaka and Rajshahi, respectively, were categorized as very high-risk zones in 2024. The very low-risk zones accounted for less than 1.5% in both cities. These findings suggested significant regional differences in urban climate risk as Dhaka was experiencing more severe circumstances, due to dense urbanization and rising pollution levels. The study unraveled the potential of GIS and remote sensing-based multi-parameter integration for urban climate risk zoning, as well as the establishment of city-specific adaptation and mitigation measures in Bangladesh.

Keywords: Urban expansion; Climate risk zones; Land surface temperature; Air pollution; Land use, Google Earth Engine

1 Introduction

Rapid urban expansion significantly alters land use patterns, particularly in developing countries, leading to profound environmental and climatic consequences [1]. The transformation of natural landscapes into built-up environments results in increased carbon emissions, climate change, unplanned urban growth, and overall environmental degradation, rendering urban areas less sustainable for human settlement [2, 3]. Urban sprawl often extends beyond planned areas, encroaching on vulnerable regions and creating climate risk zones [4]. Among the most critical consequences of this expansion is the modification of land surface temperature (LST), which has direct implications for urban climate risks, particularly through the intensification of urban heat islands (UHI) [5–7]. As urbanization progresses, UHI effects exacerbate temperature extremes, deteriorating environmental conditions and impacting public health [8, 9]. Global warming amplifies LST, with drylands experiencing up to 44% more warming than humid regions at the same increase in global temperature, leading to disproportionate climate risks for nearly 38% of the population in the world [10]. Rising temperatures and changing weather patterns increase the formation and persistence of pollutants, such as ozone and PM_{2.5}. Especially during heatwaves and stagnation events, there would be more frequent and severe air pollution episodes, thus raising mortality and morbidity rates [11–13]. Besides, rapid urban growth hinders the development of optimum housing and causes informal settlements or slums. As a result, these portions of urban areas typically lack crucial services such as clean water, sanitation, and adequate green space, which create unhygienic and miserable living conditions [14]. Being one of the most pressing concerns in urban

areas, air pollution has been exacerbated by rapid population growth, increased vehicular emissions, industrialization, and unplanned urbanization [15]. The global urban population, which was approximately 30% in 1950, surpassed 50% in 2014 and is projected to reach 60% by 2030, accounting for nearly 5 billion people [16].

Numerous studies have documented the combined effects of climate change and urbanization on rising temperatures, air pollution, and heat stress in cities worldwide. For instance, a study by Chapman et al. [17] highlighted the impact of climate change and urban growth on urban climate and heat stress in Brisbane, Australia. Abulibdeh et al. [18] illustrated the relationship among land use, LST, and carbon footprints in arid urban areas of Doha, Qatar. Their study demonstrated how rapid urbanization altered land use, leading to increased LST and higher energy consumption. Furthermore, Hien et al. [19] showcased in their studies how urban expansion played a role in altering atmospheric parameters and the impact of urban expansion on the air pollution landscape. They employed multi-regional input-output (MRIO) models to identify traffic, industrial, and residential emissions as major contributors to worsening air quality. A study by Ji et al. [20] in Asia demonstrated the changes and interrelationships between regionally eco-environmental quality and landscape pattern in the Jing-Jin-Ji (JJJ) urban agglomeration from 2001 to 2015. The combined effects of air pollution and climate change significantly increased the risk of chronic respiratory diseases, cardiovascular problems, mental health disorders, and premature death. Utilizing Shannon entropy and landscape metrics for urban sprawl studies, Aurora and Furuya [21] analyzed the relationship between urban sprawl and ecological quality in Chiba Prefecture with the spatial context of the metropolitan region. Climate risk zoning could incorporate ecosystem service mapping to inform where green infrastructure or nature-based solutions are most needed, hence supporting both adaptation and sustainability [22].

Satellite-based remote sensing approaches are indispensable for assessing LST and UHI over time and space [23]. Remote sensing, often combined with geographic information system (GIS) and probabilistic modeling, enables detailed mapping of climate risk zones for hazards like floods, droughts, and groundwater scarcity [24]. However, traditional remote sensing indices such as normalized difference vegetation index (NDVI), normalized difference water index (NDWI), soil adjusted vegetation index (SAVI), and infrared percentage vegetation index (IPVI) have shown limitations in accurately characterizing land use and land cover (LULC) categories due to spectral mixing issues [25]. These challenges arise from the complex spectral responses of different land cover types, including built-up areas, water bodies, vegetation, agricultural land, and barren lands [26]. In this regard, Google Earth Engine (GEE) has become a potent cloud-based platform for big data processing, enabling large-scale analysis of satellite imagery, without the demand for extensive computational resources [27]. GEE as a reliable tool, is capable of studying urban expansion, changes in LST, and trends of air pollution as well as assessing risk zones at high spatial and temporal resolutions. GIS is essential for conducting spatial analysis, mapping risk zones, and integrating multiple data layers of hazards, exposure, and vulnerability [28]. Multi-criteria evaluation framework combines hazard, exposure, and vulnerability indicators to produce implementable risk maps, which often adopt influence matrices and risk indices to evaluate the combined impact of multiple hazards and vulnerabilities [28, 29]. The weighted linear combination (WLC) method involves assigning a weight to each risk indicator based on its perceived importance. It then sums the weighted indicators to generate a composite risk score for each spatial unit, which allows trade-offs among criteria and could be easily administered in GIS environments [30].

Prior studies on Dhaka City Corporation (DCC) and Rajshahi City Corporation (RCC) have primarily focused on either changes in LST or trends of air pollution, thus overlooking their combined impact on climate risk zones. For instance, Ahmed et al. [31] and Rahman et al. [32] simulated LULC changes and their impact on LST in Dhaka, Bangladesh. Similarly, Zarin and Esraz-Ul-Zannat [33] investigated changes in air quality in Dhaka using Transitional Potential Modeling and Cellular Automata Simulation. Other studies, such as those by Biswas et al. [34] and Rahnuma et al. [35], examined air quality in relation to LULC changes using advanced analytical techniques like particle-induced X-ray emission (PIXE), Statgraphics, and positive matrix factorization (PMF). Meanwhile, Akash and Puja [36] assessed fluctuations of LST in LULC changes and rapidly urbanizing environments in Dhaka and Rajshahi. They emphasized the impact of urbanization on heat stress through ground-based and satellite-derived observations.

Most studies envisaged either UHI or air pollution as a pivotal problem in a city, yet there is a lack of research on combining these factors to analyze climate risks for a future sustainable city environment. Given these gaps in the existing literature, this study employed an innovative approach by integrating high-resolution remote sensing data with GEE-based cloud computing. The approach, when applied in DCC and RCC, could shed light on the combined impact of urban expansion on LST and air pollution parameters, with LULC changes over the time. Traditional studies depended on conventional GIS techniques or ground-based measurements to analyze these issues separately. Nevertheless, the current research integrated LULC, LST, air pollution parameters, and a time series analysis; it leveraged big-data analytics to delineate climate risk zones, thus achieving greater precision for DCC and RCC.

Climate risk zoning guides where and how development should occur, in order to ensure new buildings and infrastructure are sited and designed to withstand local climate hazards. This supports sustainable urban growth by balancing development needs with environmental protection. Besides, the study subsumed a weighted overlay

analysis, along with the data, to mark high-risk urban zones by considering several environmental stresses. The key objectives of this study are: (1) to analyze the spatiotemporal dynamics of urban expansion in DCC and RCC from 2020 to 2024; (2) to identify and delineate climate risk zones linked to temperature and air pollution stress; and (3) to examine the interrelationship between urban expansion and climate risk zones. The findings will bridge existing research gaps, inform urban sustainability strategies, and contribute to effective mitigation and adaptation measures in rapidly expanding cities.

2 Materials and Method

2.1 Study Area

The present study focused on DCC and RCC (Figure 1).

DCC: Dhaka is one of the fastest expanding mega cities of Bangladesh. Situated between $23^{\circ}41'N$ to $23^{\circ}55'N$ latitude and $90^{\circ}20'E$ to $90^{\circ}30'E$ longitude, DCC is the most populated city in the country. The city consists of two administrative divisions, Dhaka North City Corporation (DNCC) and Dhaka South City Corporation (DSCC). DNCC comprises 54 wards, covering areas such as Mirpur, Gulshan, and Uttara, while DSCC consists of 75 wards, covering regions including Paltan, Motijheel, and Dhammondi [37]. The current population of DCC is over 10.2 million, with DNCC having 5.98 million and DSCC having 4.3 million residents [38]. The city has witnessed rapid urbanization and extreme LULC change with built up expansion, encroaching upon vegetation and water bodies [39]. The process has directly impacted LST, which drives the UHI effect, resulting in higher temperatures, increased energy demand, and less environmental sustainability [40].

RCC: Rajshahi is located in the northwestern part of Bangladesh. Geographically, it spans between $24^{\circ}20'N$ and $24^{\circ}24'N$ latitude and $88^{\circ}32'E$ and $88^{\circ}40'E$ longitude, encompassing an area of 95.56 km^2 [41]. The city is situated on the north bank of the Padma River near the Bangladesh-India border, and is surrounded by the satellite towns of Nowhata and Katakhali [42]. The current population of RCC is over half a million. Rajshahi, the “Silk City” of Bangladesh, is the hub of the textile industry and has experienced unprecedented LULC changes in the recent decades. The residential, commercial, and industrial growth has expanded the urban area by transforming agricultural land and open spaces into built-up land [43]. The rapidly evolving LULC has significantly impacted LST, where studies revealed a strong correlation between urban growth and rising temperatures, with consequential thermal discomfort and environmental degradation [44].

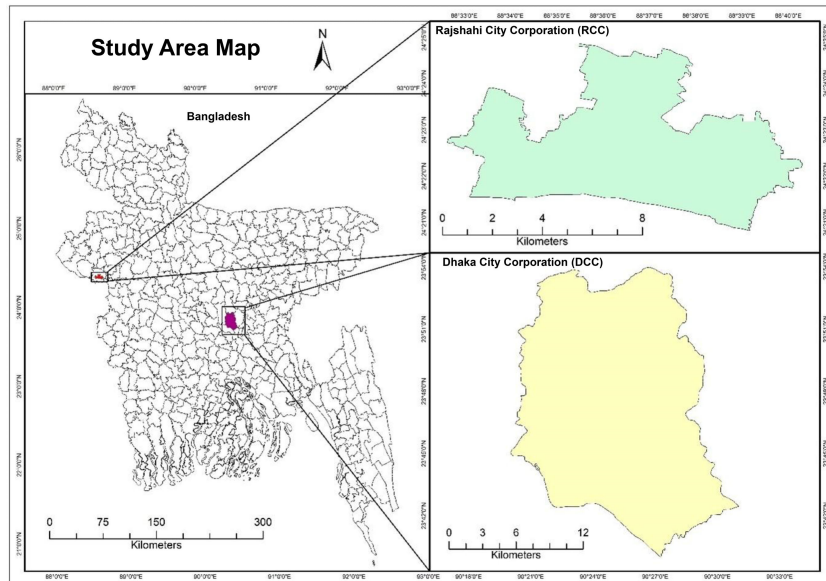


Figure 1. Locations of the study areas, DCC and RCC

Our research focused on DCC and RCC, since they are more vulnerable to climate-related concerns. DCC, the capital of Bangladesh, has severe floods, heatwaves, and air pollution. Over 60% of Dhaka was built-up with low vegetation and water bodies, thus intensifying the UHI effect and heightening its vulnerability to heatwaves, which adversely harm public health and infrastructure [45, 46]. Similar to this situation, RCC is vulnerable to high temperatures, as the built-up area in the city expanded by over 53% from 1992 to 2022. The UHI effect was intensified by the dramatic decline in green cover, which reduced the thermal comfort zones [47, 48]. Demarcating the climate risk zones in these cities is critical for establishing tailored adaptation and mitigation measures to boost resilience and sustainability.

2.2 Description of the Data

Satellite imagery of 2020 and 2024 for conducting LULC (Table 1) and estimating LST (Table 2) respectively, was obtained from GEE and the United States Geological Survey (USGS) Earth Explorer. The years have been chosen on the basis of the acceleration of urbanization trend, emerging climatic shifts, and data availability. The cloud cover was less than 15%.

Table 1. Description of the images used for conducting LULC

Study Area	Satellite Data	Date of Acquisition	Sensor	Military Grid Reference System (MGRS)	Band No.	Central Wavelength (μm)	Spatial Resolution (m)
DCC	Sentinel 2A	17 April 2020	MSI	100 km/100 km	2	0.490	10
					3	0.560	10
					4	0.665	10
					8	0.833	10
					8A	0.865	20
					11	1.613	20
					12	2.190	20
					2	0.490	10
					3	0.560	10
					4	0.665	10
RCC	Sentinel 2A	16 April 2024	MSI	100 km/100 km	8	0.833	10
					8A	0.865	20
					11	1.613	20
					12	2.190	20
					2	0.490	10
					3	0.560	10
					4	0.665	10
					8	0.833	10
					8A	0.865	20
					11	1.613	20
Sentinel 2A	15 April 2020	MSI	100 km/100 km		12	2.190	20
					2	0.490	10
					3	0.560	10
					4	0.665	10
					8	0.833	10
Sentinel 2A	4 May 2024	MSI	100 km/100 km		8A	0.865	20
					11	1.613	20
					12	2.190	20

Note: MSI: multispectral imager

2.3 Image Preprocessing

Atmospheric correction of images from Sentinel 2A was done utilizing GEE to minimize radiometric distortions. The Sentinel-2 cloud mask (SCL) band was adopted to identify and exclude cloudy pixels from the analysis, thus ensuring the accuracy of LULC classifications. Temporal and spatial averaging were performed to reduce noise and enhance signal quality in the air pollution data.

2.4 Estimation of LST

LST was estimated in ArcGIS 10.8 from Landsat 8 imagery using the Mono-Window Algorithm (MWA), which requires several key parameters:

Top-of-Atmosphere ($L\lambda$) [49]:

$$L\lambda = M_L \times Q_{CAL} + A_L \quad (1)$$

where, M_L = Radiance multiplicative scaling factor (from metadata *RADIANCE_MULT_BAND_10*; -0.00003342); A_L = Radiance additive scaling factor (from metadata: *RADLANE_ADD_BAND_10*; -0.0010); Q_{CAL} = Quantized and calibrated standard product pixel value (DN).

Table 2. Description of the images used for estimating LST

Study Area	Satellite Data	Date of Acquisition	Sensor	Path/Row	Band No.	Spectral Range (μm)	Spatial Resolution (m)
DCC	Landsat 8	30 March 2020	OLI	137/44	4	0.64–0.67	30
					5	0.85–0.88	30
					10	10.6–11.19	60
RCC	Landsat 8	26 April 2024	OLI	137/44	4	0.64–0.67	30
					5	0.85–0.88	30
					10	10.6–11.19	60 (resampled to 30)
RCC	Landsat 8	6 April 2020	OLI	137/44	4	0.64–0.67	30
					5	0.85–0.88	30
					10	10.6–11.19	60 (resampled to 30)
RCC	Landsat 8	3 May 2024	OLI	137/44	4	0.64–0.67	30
					5	0.85–0.88	30
					10	10.6–11.19	60 (resampled to 30)

Note: OLI: optical land imager

Brightness Temperature (BT) [50]:

$$BT = \frac{K_2}{\ln\left(\frac{K_1}{L_\gamma} + 1\right)} - 273.15 \quad (2)$$

where, $K_1 = 774.89 \text{ W/m}^2/\text{sr}/\mu\text{m}$; $K_2 = 1321.08 \text{ K}$.

Normalized Difference Vegetation Index (NDVI) [51]:

$$NDVI = \frac{NIR - RED}{NIR + RED} \quad (3)$$

where, NIR = Near Infrared; NIR and RED represent the B4 and B5 bands, respectively.

Proportion of Vegetation (Pv) [43]:

$$P_v = \left(\frac{NDVI - NDVI_{min}}{NDVI_{max} - NDVI_{min}} \right)^2 \quad (4)$$

where, Pv = Proportion of Vegetation; $NDVI$ = DN values from NDVI Image; $NDVI_{min}$ = Minimum DN values from NDVI Image; $NDVI_{max}$ = Maximum DN values from NDVI Image.

Land Surface Emissivity (LSE) [52]:

$$LSE = 0.004 \times Pv + 0.986 \quad (5)$$

where, 0.986 corresponds to a correction value of the equation.

Final LST Calculation [53]:

$$LST = \frac{BT}{1 + \left(\frac{\lambda \times BT}{C_2} \right) \times \ln(E)} \quad (6)$$

where, λ is the wavelength of emitted radiance (approximately $10.8 \mu\text{m}$ for Band 10); C_2 is the second radiation constant (approximately $14,388 \mu\text{m K}$); E is the land surface emissivity (LSE).

2.5 LULC Classifications

Supervised classification was conducted in GEE using the Random Forest (RF) classifier, a machine learning algorithm with high precision in LULC mapping [54]. Training samples were collected for five major land cover classes: waterbody, vegetation, built-up area, barren land, and agricultural land (Table 3).

A total of 200 training samples were obtained for each class of the two study areas separately for classification. The classifier was trained on labeled samples with an equal number of decision trees to enhance classification accuracy.

Table 3. Description of the LULC classes

LULC Classes	Description
Waterbody	Areas seasonally or permanently covered with water, including lakes, rivers, ponds, wetlands, and reservoirs.
Vegetation	Land dominated by natural or planted green cover, such as forests, small trees, shrubs, and tree canopies, etc.
Built-up area	Urban, peri-urban, or semi-urban areas built with man-made structures, such as buildings, factories, roads, and other small settlements.
Barren land	Exposed soil, sand, rocks, or arid land with little to no vegetation cover.
Agricultural land	Areas used for systematic crop cultivation and farming activities, including irrigated and rainfed fields.

2.6 Assessment of Accuracy

An error matrix was produced, and such important parameters as Overall Accuracy (OA) and Kappa coefficient were derived for the accuracy assessment [55]. Independent validation points were randomly chosen from high-resolution images and cross-checked with the classified raster. The number of random points used in the procedure of conducting the accuracy assessment was 50 for each of the years of DCC and RCC, and the sample strategy used in this process was “Stratified Random”.

2.7 Change Detection

Post-classification comparison was performed to assess LULC changes among 2016, 2020, and 2024. Classified maps were superimposed, and area statistics were computed to quantify changes of land cover class over the time. Temporal trends were analyzed to detect urban expansion in DCC and RCC.

2.8 Analysis of Air Pollution

To evaluate the air quality of DCC and RCC, four key atmospheric pollutants, i.e., NO₂, SO₂, CO, and PM_{2.5} were selected as indicators, due to their strong association with anthropogenic activities, including vehicular emissions, industrial processes, and energy consumption, which are recognized as major contributors to urban climate risks.

The estimation of pollutant concentrations was carried out using GEE, which provides an efficient cloud-based platform for processing multi-source atmospheric datasets. Sentinel-5P TROPOMI products were utilized to extract column concentrations of NO₂, SO₂, and CO, while the NASA GEOS-CF v1 Reanalysis dataset was employed to estimate surface-level PM_{2.5} concentrations at hourly temporal resolution. The datasets were filtered for the study period from year 2020 to 2024. To capture the peak air pollution period, the analysis was restricted to winter (November to December), when atmospheric stability, reduced height of boundary layers, and increased emissions typically result in elevated pollution levels across Bangladeshi cities. The pollutant layers were then spatially clipped to the administrative boundaries of DCC and RCC to facilitate inter-city comparability. Monthly composites were generated to represent the seasonal conditions, and seasonal means were calculated for subsequent analysis.

2.9 Climate Risk Zone Mapping

To delineate urban climate risk zones in DCC and RCC, a multi-criteria evaluation (MCE) framework was employed using the six selected indicators: LULC, LST, NO₂, SO₂, CO, and PM_{2.5}. These variables were integrated through a weighted linear combination (WLC) method, where each indicator was assigned a relative weight according to its influence on urban climate risk. Weights for each class of LULC was given as per Table 4.

With the weighted linear combination, factors are combined by applying a weight to each, followed by a summation of the results to yield a suitability map [56]:

$$S = \sum w_i x_i \quad (7)$$

where, S is suitability, w_i is weight of factor i , and x_i is the criterion score of factor i .

Weights were determined hypothetically based on scientific relevance from the literature on urban heat, air pollution, and public health outcomes (Table 5). Thermal stress (represented by LST) and PM_{2.5} were assigned the highest weights due to their strong association with human health and climatic extremes [57]. LULC was given a moderate weight, in recognition of its role in mediating both thermal response and pollution dispersion [58]. Gaseous pollutants, NO₂, SO₂, and CO were weighted somewhat lower, to reflect their localized but still significant impact on air quality and climate risks.

Figure 2 shows the overall workflow of the methodology undergone to conduct the research.

Table 4. Risk categories of LULC classes

LULC	Risk Category
Waterbody	1
Built-up area	5
Vegetation	2
Agricultural-land	3
Barren land	4

Table 5. Weights assigned for each parameter

Parameter	Weight	Rationale
LULC	20	Urban areas contributed to heat island effects.
LST	25	High LST correlated with climate risks.
NO ₂	15	Major pollutant affecting air quality.
SO ₂	10	Pollutant contributing to acid rain and affecting climate.
CO	10	Indicator of incomplete combustion, linked to urban pollution.
PM _{2.5}	10	Significant health and environmental hazard.

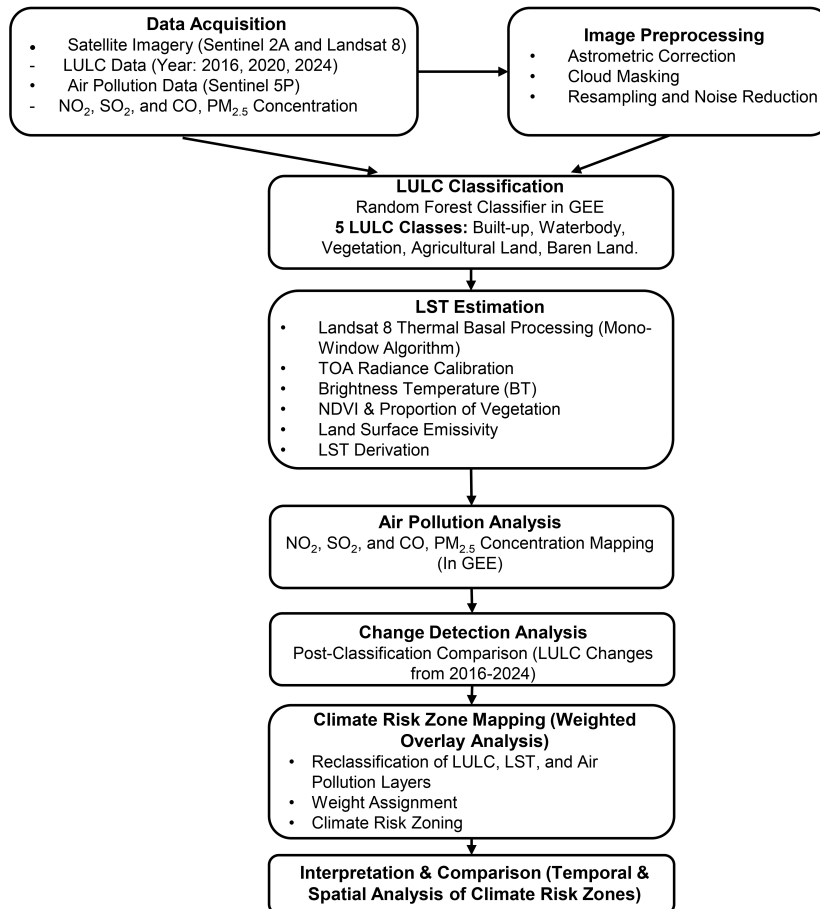


Figure 2. Methodological workflow for climate risk zoning of DCC and RCC

3 Results

3.1 Urban Expansion Patterns

Before analyzing the LULC maps, an accuracy assessment of each year has been conducted to validate the classification results in Table 6. The overall accuracy for the two listed years of DCC and RCC was more than 90%; the Kappa coefficient was more than 0.89 (Table 6).

The findings showed that built-up areas increased significantly throughout the research period, whereas vegetation,

waterbody, and agricultural land decreased (Table 7).

The categorization results demonstrated that urban expansion has been more prominent in DCC than RCC (Figure 3). In DCC, the built-up area, which displaced green spaces and wetlands, has grown dramatically. RCC, in comparison, showed a more gradual shift, with agricultural land conversion serving as the principal engine of urban expansion. The statistical study revealed a greater yearly urban expansion rate in DCC.

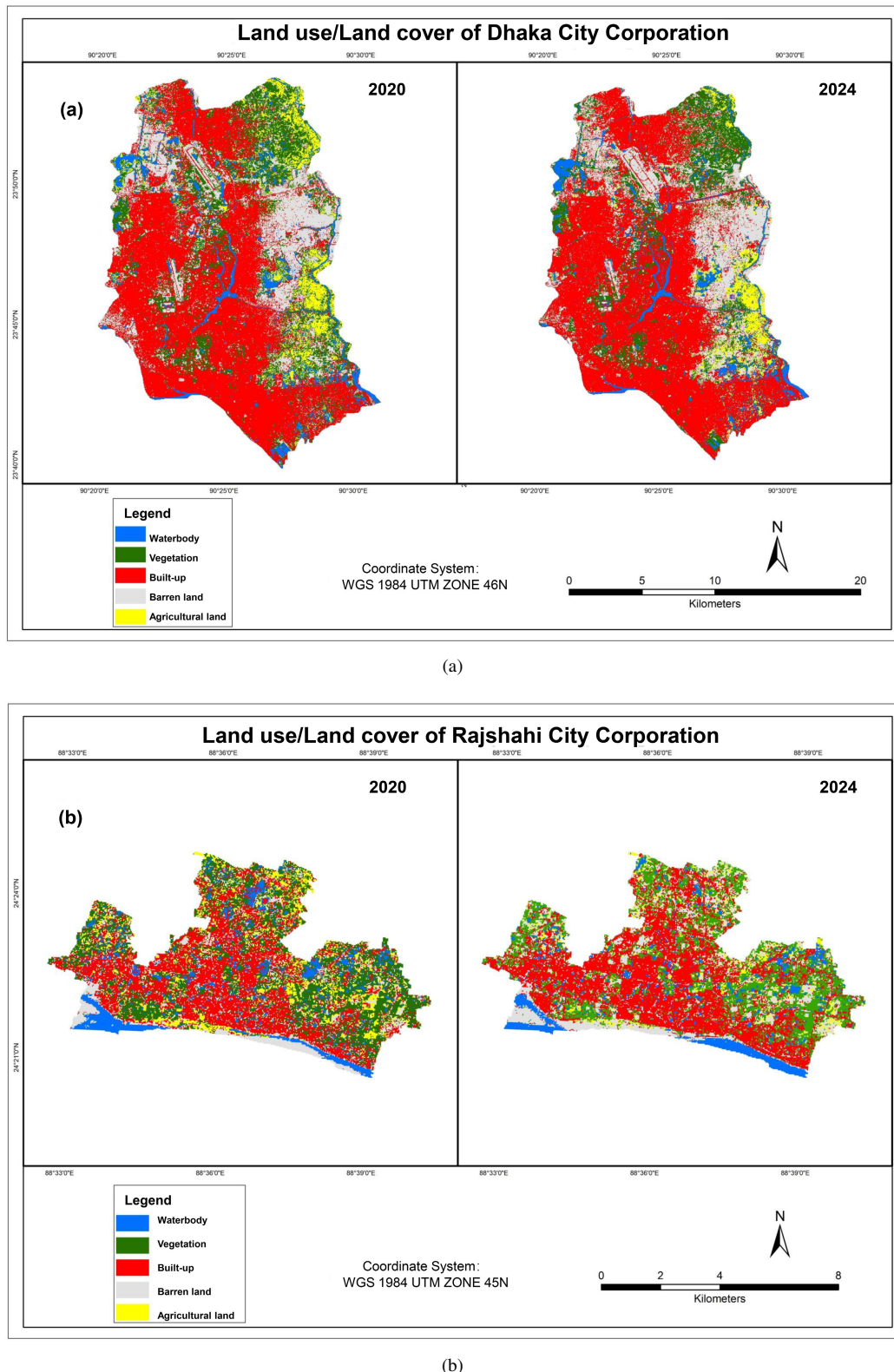


Figure 3. LULC in 2020 and 2024: (a) DCC; (b) RCC

Table 6. Results of the accuracy assessment of LULC classification

Study Area		DCC		RCC	
	Year	2020	2024	2020	2024
User accuracy (%)	Waterbody	90	100	90	100
	Vegetation	80	100	100	92.31
	Built-up	95.83	96.15	100	95.24
	Barren land	100	90.91	80	90
	Agricultural land	90	70	80	90
Producer accuracy (%)	Waterbody	90	90.91	100	100
	Vegetation	100	83.33	93.75	100
	Built-up	100	96.15	85	95.24
	Barren land	76.92	90.91	88.89	75
	Agricultural land	90	100	100	100
Overall accuracy (%)		92.18	92.53	91.94	93.75
Kappa coefficient		0.89879	0.90124	0.89680	0.91972

Table 7. LULC changes of DCC and RCC

LULC	DCC			RCC		
	Area in 2020 (%)	Area in 2024 (%)	Changes (%)	Area in 2020 (%)	Area in 2024 (%)	Changes (%)
Waterbody	6.78	6.54	-0.24	11.29	9.15	-2.14
Vegetation	19.98	16.51	-3.47	30.4	24.78	-5.62
Built-up area	47.17	51.55	4.38	31.78	40.69	8.91
Barren land	20.01	21.44	1.43	15.48	20.87	5.39
Agricultural land	6.06	3.96	-2.1	11.05	4.51	-6.54

3.2 LST Variability

The temporal analysis showed an increase in LST from 2020 to 2024 (Figure 4). The highest recorded LST values, illustrating the influence of urbanization and land cover changes, were found in both cities in 2024. A comparative analysis of LST with LULC categories demonstrated that built-up areas consistently exhibited substantially greater temperatures than vegetation and water bodies.

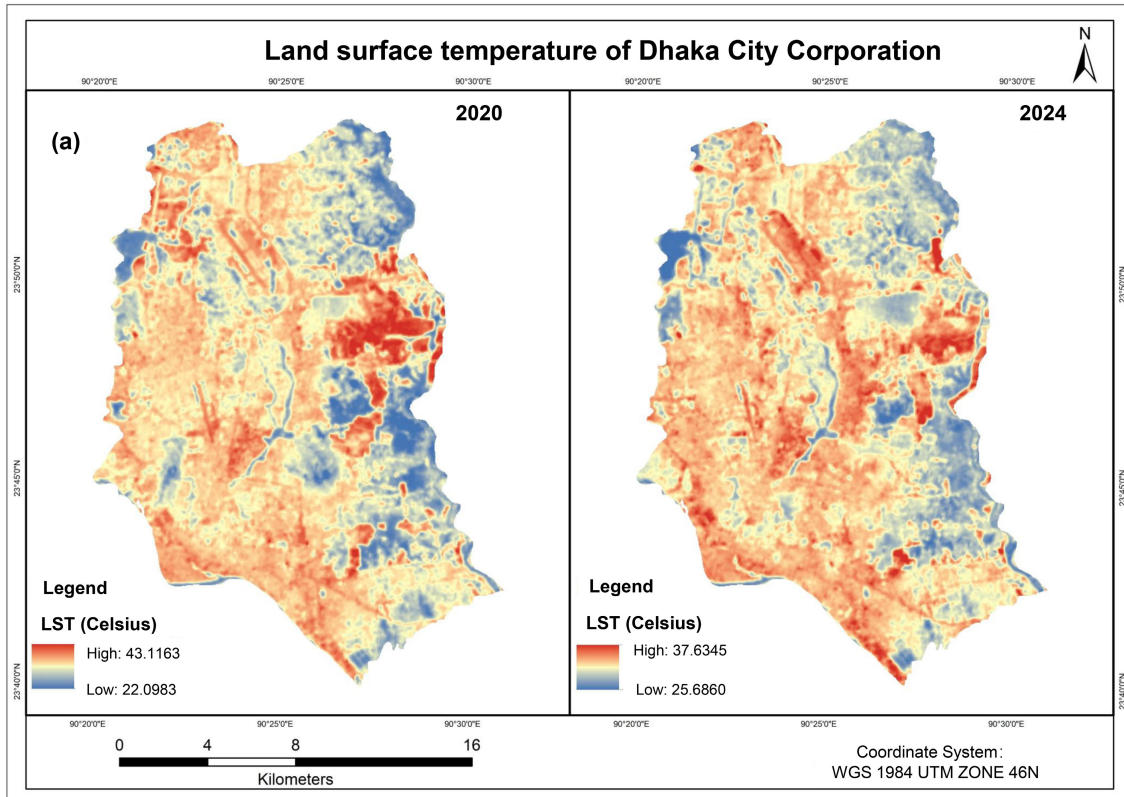
3.3 Analysis of Air Pollution

The concentrations of all four pollutants in DCC depicted a scenario of deteriorating air quality (Figure 5). The mean NO₂ concentration increased from 28.3 μmol/m² in 2020 to 36.4 μmol/m² in 2024, with the highest intensities clustered along major traffic corridors and industrial hubs. The level of SO₂ rose slightly from 11.5 μmol/m² in 2020 to 14.95 μmol/m² in 2024, with persistent hotspots in southern and western zones dominated by brick kilns and industrial facilities. The concentration of CO also showed a minor increase from 0.049 mol/m² in 2020 to 0.051 mol/m² in 2024, with higher values detected in central Dhaka and peri-urban expansion areas. On the other hand, the mean concentration of PM_{2.5} decreased from 185.53 μg/m³ in 2020 to 139.78 μg/m³ in 2024 (Table 8).

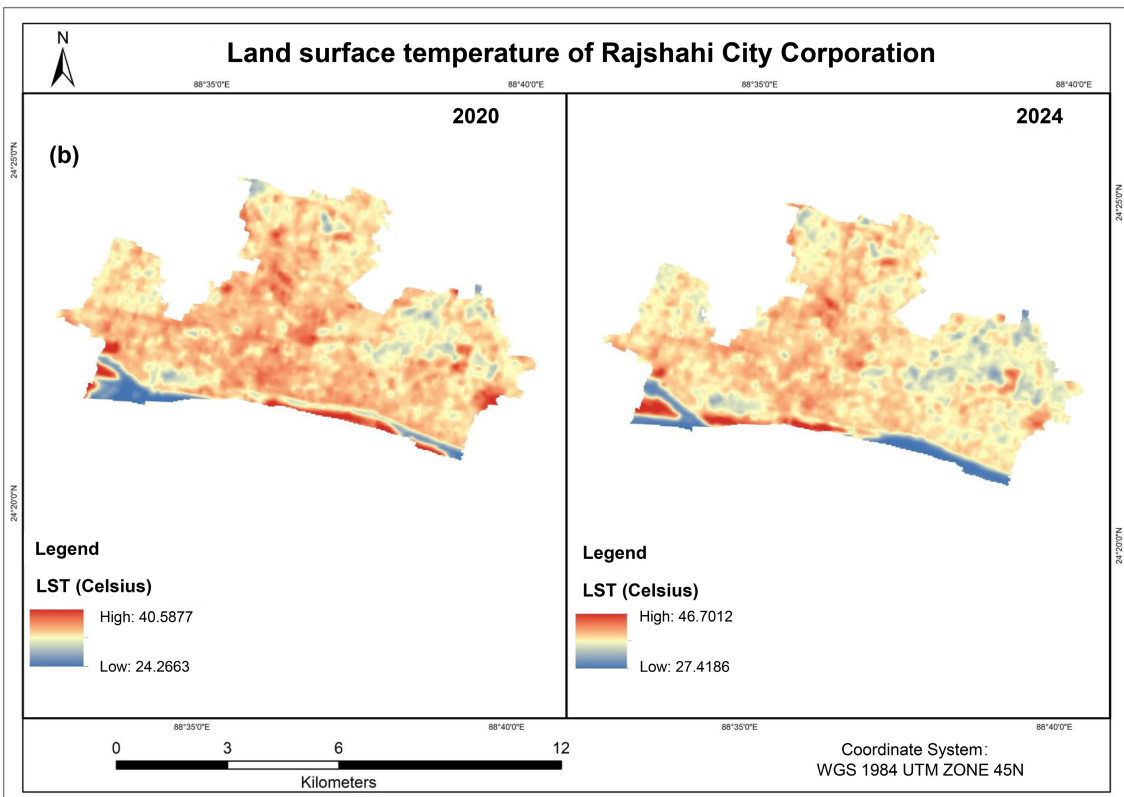
Table 8. Mean concentrations of air pollutants in DCC and RCC in year 2020 and 2024

City	Year	NO ₂ (μmol/m ²)	SO ₂ (μmol/m ²)	CO (mol/m ²)	PM _{2.5} (μg/m ³)
DCC	2020	28.3	11.5	0.049	185.53
	2024	36.4	14.95	0.051	185.53
RCC	2020	9.03	12.5	0.049	205.8
	2024	9.81	20.8	0.051	169.59

RCC demonstrated comparatively lower concentrations of all pollutants but displayed an upward trajectory (Figure 6) similar to Dhaka. NO₂ increased from 9.03 μmol/m² in 2020 to 9.81 μmol/m² in 2024, particularly concentrated in central transport corridors. The level of SO₂ was relatively modest, rising from 12.5 μmol/m² to 20.8 μmol/m² over the study period, with hotspots emerging in industrial peripheries. The concentration of CO in RCC showed a minor increase from 0.049 mol/m² in 2020 to 0.051 mol/m² in 2024, while the concentration of PM_{2.5} exhibited a decrease from 205.8 μg/m³ in 2020 to 169.59 μg/m³ in 2024, still higher than that in DCC (Table 8).



(a)



(b)

Figure 4. LST variability in the years 2020 and 2024: (a) DCC; (b) RCC

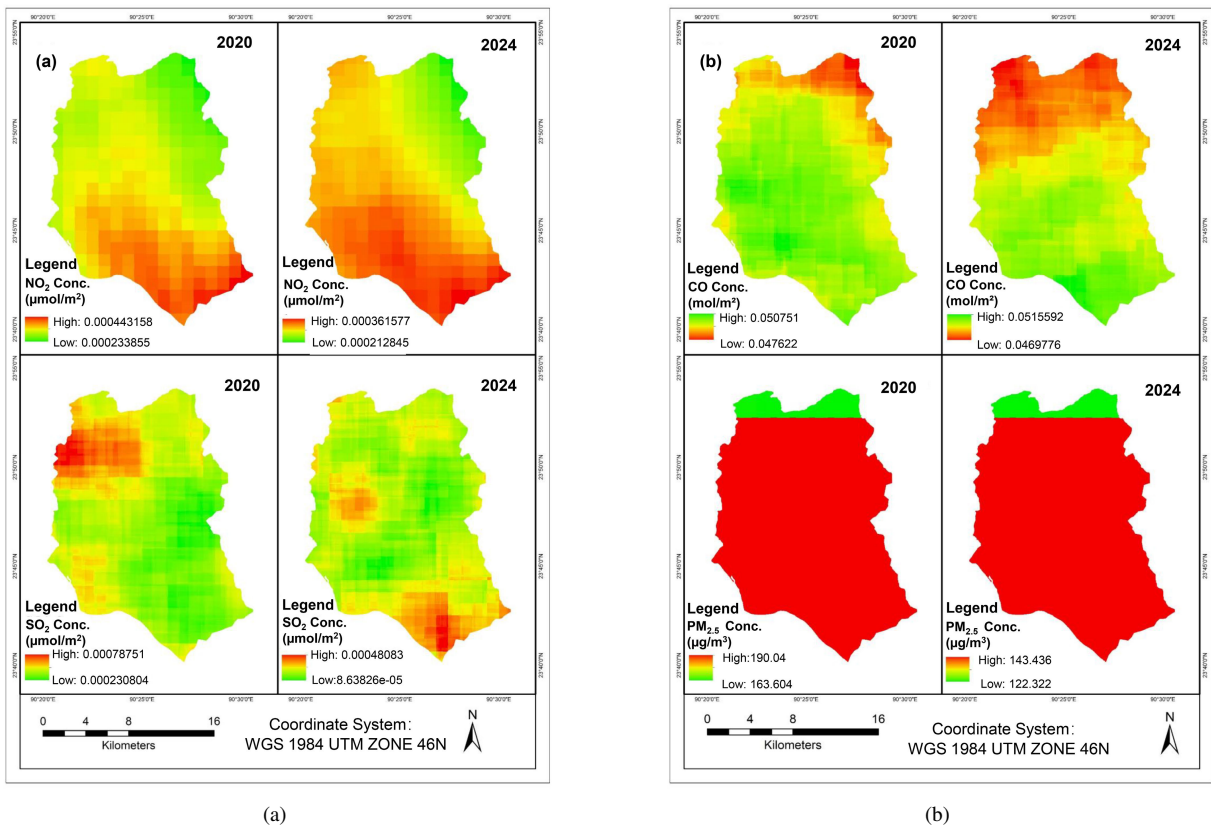


Figure 5. Pollutants in DCC for years 2020 and 2024: (a) Concentrations of NO₂ and SO₂; (b) Concentrations of CO and PM_{2.5}

3.4 Identification of Climate Risk Zones

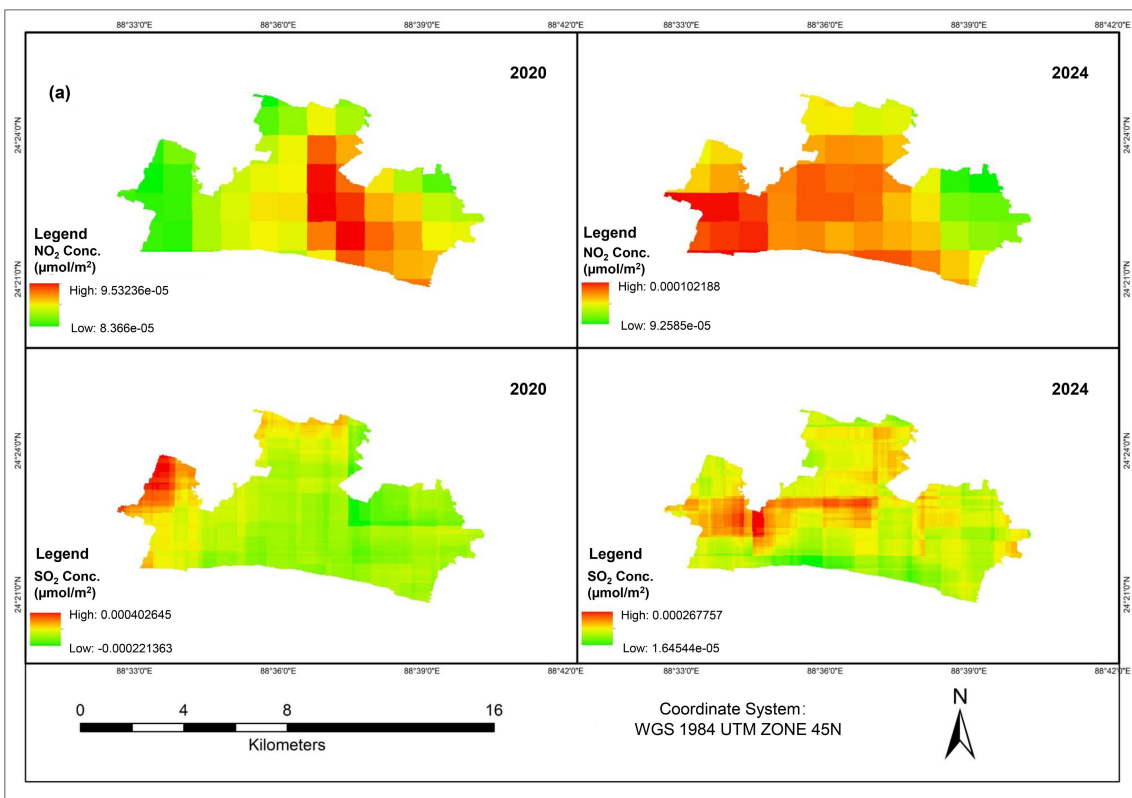
The climate risk zones were divided into five categories: very low, low, moderate, high, and extremely high risk (Table 9). The spatial distribution and proportion of regions falling into each category in DCC and RCC were examined for year 2020 and 2024.

Table 9. Changes in the climate risk zones of DCC and RCC

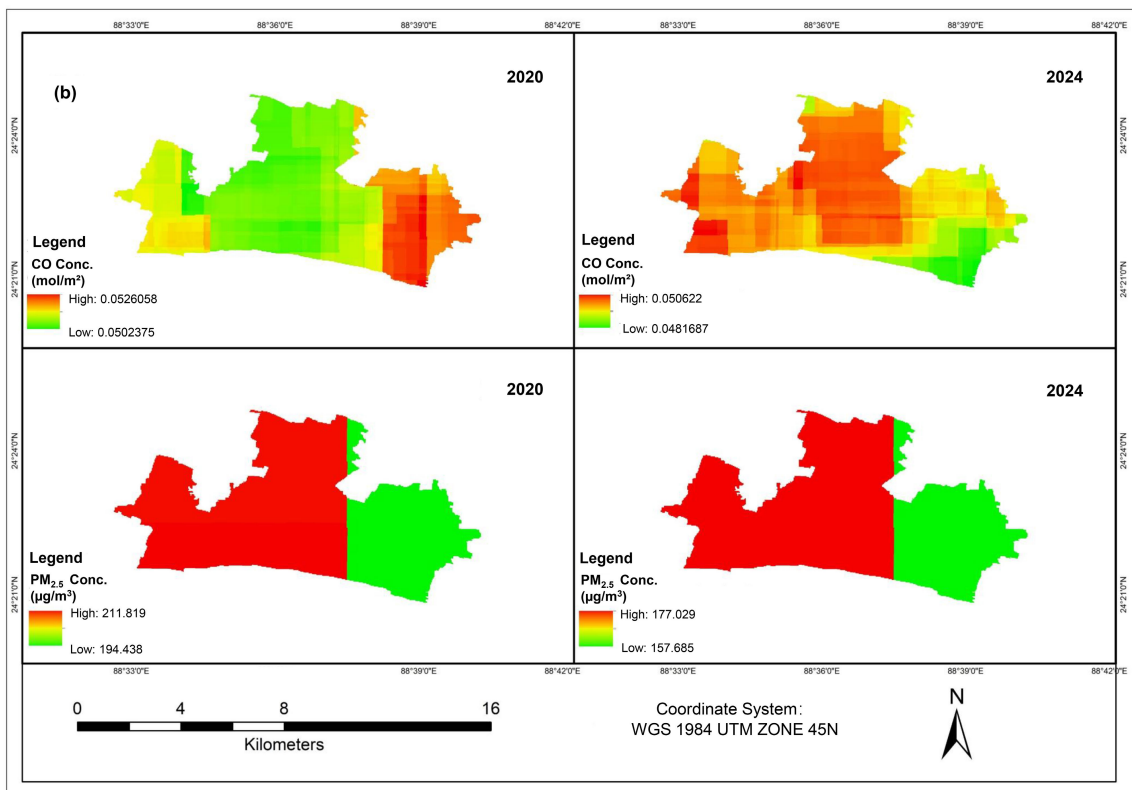
Risk Zones	DCC		RCC	
	Area in 2020 (%)	Area in 2024 (%)	Area in 2020 (%)	Area in 2024 (%)
Very low	1.04	1.48	0.004	0.54
Low	18.38	17.46	20.251	21.80
Moderate	44.03	42.53	70.255	39.34
High	35.93	33.16	9.490	36.69
Very high	0.61	5.38	—	1.63

The moderate-risk zone remained dominant in DCC throughout the research though its extent dropped slightly, as additional places moved into higher-risk categories. The high-risk zone, while still encompassing a substantial portion of the city, was also on the decline. However, the most alarming trend could be visualized in the very high-risk category, which increased considerably in 2024 compared to 2020, thus implying a rise in severe urban area and air pollution levels. Meanwhile, the very low and low-risk zones showed slight variations, indicating localized improvements in environmental circumstances in some places (Figure 7).

In RCC, the most striking development was the significant decline in the moderate-risk zone, which once encompassed a large area of the city but had shrunk significantly by 2024. This transition was followed by a significant rise in high-risk locations, indicating increased environmental stress. Furthermore, the emergence of a previously undetected very high-risk zone highlighted the rising climate vulnerability in certain areas of the city (Figure 8).



(a)



(b)

Figure 6. Pollutants of RCC for years 2020 and 2024: (a) Concentrations of NO₂ and SO₂; (b) Concentrations of CO and PM_{2.5}

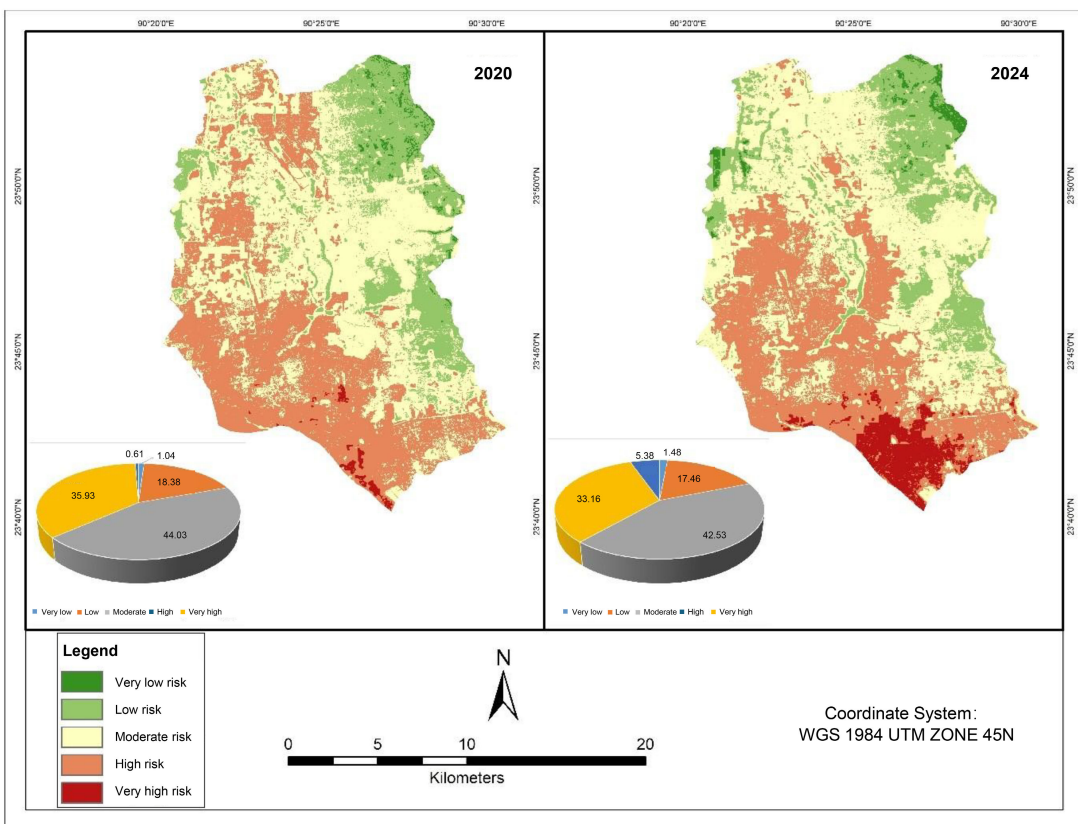


Figure 7. Climate risk zones of DCC for years 2020 and 2024

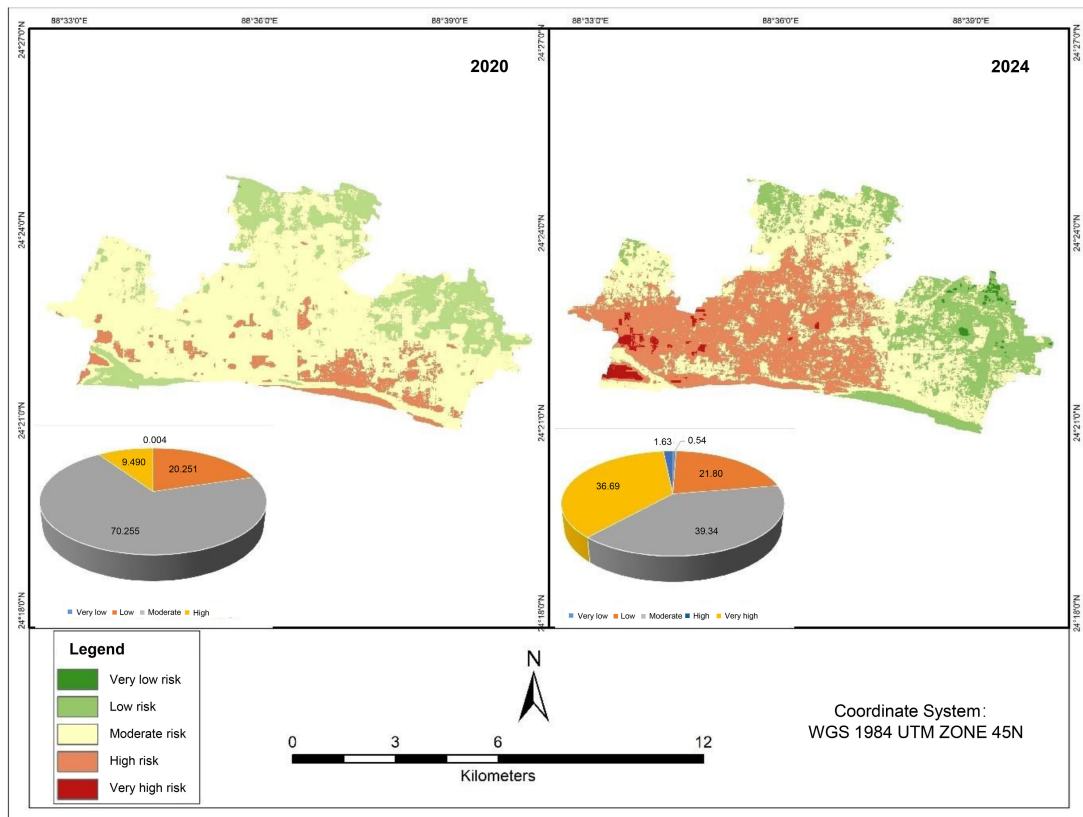


Figure 8. Climate risk zones of RCC for years 2020 and 2024

3.5 Nexus Between Urban Area and Climate Risk Zones

The investigation of urban growth and climate risk zones in DCC and RCC showed a substantial link between rapid urbanization and increased climate vulnerability. The geographical overlay of changes in LULC with climate risk zones showed that built-up areas increased at the expense of vegetation cover and water bodies, resulting in higher LST and poorer air quality.

In DCC, intensely urbanized regions correspond to high and extremely high-risk zones. The loss of green areas and wetlands has increased surface heat absorption, thus aggravating the impact of UHI.

A comparable pattern, but with a somewhat lesser intensity, is seen in RCC. High-risk areas have increased as a result of urban growth, especially along commercial and transit routes in the city.

3.6 Comparison Between DCC and RCC

3.6.1 Urban expansion

Compared to RCC, DCC, as the capital city, showed a far greater magnitude of urban growth. The usually fast urbanization and population expansion were reflected in the substantially larger increase in built-up areas in DCC. Approximately 18% more land was covered by built-up regions, which replaced formerly vegetated and agricultural land.

In contrast, RCC had a very moderate growth in built-up areas, increasing by around 10% throughout the same period. This suggested a slower rate of urbanization than DCC, most likely as a result of slower population growth and other socioeconomic variables (Figure 9).

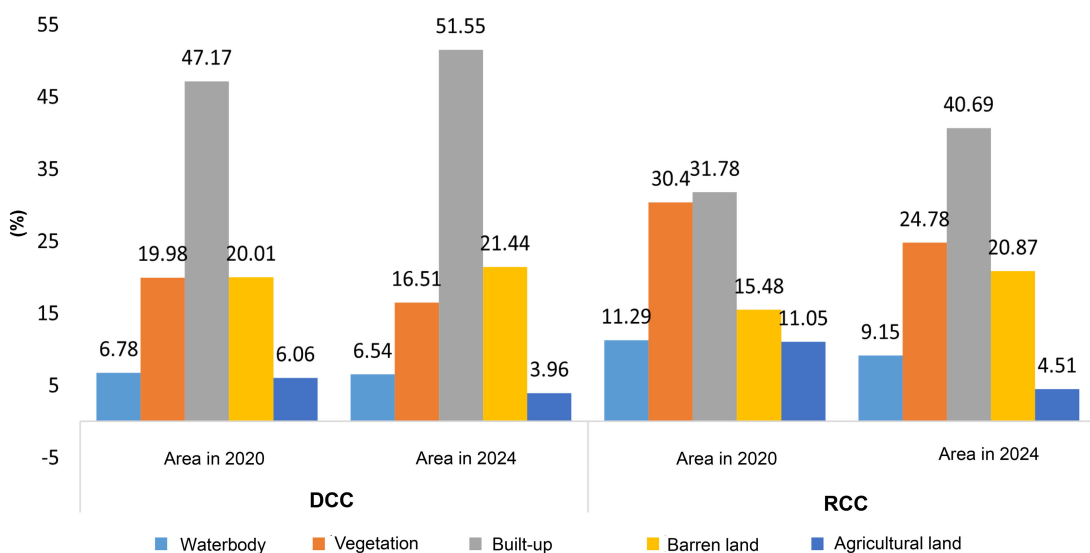


Figure 9. Comparison of LULC between DCC and RCC from year 2020–2024

3.6.2 LST & pollution

Due to its accelerating urbanization, DCC saw a significant rise in LST, with UHIs becoming more noticeable in 2024. This indicated that DCC was more susceptible to climate threats, especially when densely populated places paired with greater levels of air pollutants like NO₂, SO₂, CO, and PM_{2.5}.

RCC also showed an increase in LST over the same period, but the growth was less pronounced, and air pollution levels were relatively lower compared to DCC. The distribution of low to moderate risk zones in RCC indicated a relatively better environmental condition despite urban expansion.

3.6.3 Climate risk zones

Owing to the intensifying UHI effect and the densification of built-up regions, DCC experienced a larger percentage of high and extremely high-risk zones, especially in 2024. The moderate-risk zones in DCC somewhat shrank, thus indicating that the recently urbanized regions were more susceptible to the effects of climate change caused by increased pollution and heat.

With a higher percentage of low- and moderate-risk locations, RCC had a more evenly distributed risk zone. In 2024, however, there was a notable rise in high-risk areas, mostly as a result of land cover changes and urbanization.

4 Discussion

Two significant Bangladeshi cities, DCC and RCC, were investigated to unveil a thorough evaluation of the relationships among urban growth, LST, and air pollution, as well as how these factors collaborate in order to delineate climate risk zones. The results unequivocally showed that, especially in DCC, where urbanization has proceeded at a far more aggressive rate, fast urban expansion was substantially correlated with rising LST and declining air quality.

The growth in climate risk zones that coincides with the expansion of built-up area in DCC (4.38%) and RCC (8.91%) between 2020 and 2024 supported earlier findings that urban sprawl exacerbated the effects of UHI and environmental degradation [6, 49]. The severity and distribution of dangers are where the cities diverge most. Denser development and substantial vegetation loss characterize DCC, which exhibits an explicit movement toward high and extremely high-risk zones. This is consistent with the research by Ahmed et al. [31] and Zarin and Zannat [33], they found that the densely populated areas in Dhaka were hotspots for air pollution and UHI concerns. These findings align with global research that emphasized the compounding consequences of urbanization, land conversion, and climatic stress in places like Guangzhou in China and Hanoi in Vietnam [7, 19]. More than 60% of Dhaka is built-up, correlating with high LST and robust UHI effects. High- and very high-risk heat zones are concentrated in areas with dense built-up land and low vegetation, especially in the southern and central city [46, 59].

RCC, on the other hand, shows a gradual but notable transformation. As rural lands transformed into built-up regions, moderate-risk zones moved toward higher-risk categories, especially along industrial belts and transportation corridors [36, 41, 42]. The developing risk environment in RCC reflected that cities with slow development might still be prone to climate vulnerability.

The integrated climate risk zoning technique integrates LULC, LST, and several air pollutants like NO₂, SO₂, CO, and PM_{2.5} with a weighted overlay analysis. This is one of the main innovations lacking in urban studies conducted in Bangladesh. Although earlier studies concentrated on either LST [24, 31] or air quality [34, 35, 60], few have addressed their synergistic effects on defining climate risk zones across time. Effective risk reduction requires incorporating climate adaptation into urban planning, such as resilient infrastructure, green spaces, and flood protection systems. Cities with proactive planning (e.g., Amsterdam) fare better than those with reactive or inadequate measures (e.g., Houston) [61]. Accelerated urbanization of a city, if not adequately managed, may greatly heighten its vulnerability to climate-related dangers in view of rising temperatures and degraded air quality. The growth in high-risk and extremely high-risk zones in DCC and RCC urges for the incorporation of climate risk assessments into urban design. Expanding urban green spaces, optimizing land use, and integrating LST data into planning could mitigate heat risks and enhance resilience [62].

Using GEE for multi-temporal LST extraction and LULC classification improves the scalability and accuracy of analysis, in order to provide a methodological advancement in conventional GIS-based research [63]. This study emphasized how risk categories were dynamically redistributed over the time. An increasing trajectory of climate vulnerability was depicted by the considerable expansion in extremely high-risk zones in DCC (from 0.61% to 5.38%) and RCC (from 0% to 1.63%) by 2024. Even secondary cities like RCC are susceptible to compounded urban climate hazards [45, 47].

To counteract the impact of UHI and LST, cities should emphasize green infrastructure such as parks, green roofs, and urban trees [64]. Previous research indicated that urban greening and improved land use planning could reduce the impact of UHI and pollutant loads [9, 44, 51]. However, the implementation of greening in the developing DCC remains to be limited, owing to minor integration of climate-adaptive infrastructure.

This study contributed to the current body of knowledge by combining several environmental indicators and providing a reproducible framework for climate risk zoning in rapidly urbanizing areas. The weighted overlay technique provides policymakers with an obvious and spatially explicit framework to determine priority intervention zones for urban resilience planning. By devising detailed and spatially explicit risk maps, climate risk zoning enables city planners and policymakers to make informed decisions, revise zoning plans, and impose interventions that enhance urban resilience.

5 Conclusions

This study presented a detailed spatiotemporal evaluation of urban development, LST fluctuation, and air pollution levels in DCC and RCC, with a focus on their influence on climate risk zones. Having adopted GIS and remote sensing techniques, this study illustrated a substantial link between growing urbanization and climate risks, thus calling for sustainable urban planning and climate adaptation solutions.

The expansion of built-up regions has increased their exposure to high heat, air pollution, and environmental degradation, rendering cities more vulnerable to climate-related health and infrastructure issues. The findings underscored the need of incorporating climate risk assessments into urban planning frameworks in order to prevent negative consequences and strengthen urban resilience.

To tactfully address these issues, legislators and urban planners should prioritize sustainable land use policies, green infrastructure development, and stricter air quality control. Implementing nature-based solutions, such as urban trees, green roofs, and water conservation measures, could assist in attenuating the UHI effect and alleviating environmental stress. Strong adherence to the legislation of emission control, promotion of public transportation, and use of sustainable energy sources may considerably enhance air quality and overall urban livability. By inference, this study advocated proactive urban planning and environmental management in rapidly urbanizing cities, such as Dhaka and Rajshahi. GIS and remote sensing technology could help city administrators and politicians establish better informed and climate-resilient policies with ease for ensuring long-term urban expansion, while simultaneously protecting public health and environmental stability.

Author Contributions

Conceptualization, T.S. and M.I.T.; methodology, T.S., M.I.T. and M.A.; software, T.S., M.I.T. and M.A.; validation, T.S.; formal analysis, T.S.; investigation, T.S.; resources, T.S., M.I.T. and M.A.; data curation, T.S., M.I.T. and M.A.; writing—original draft preparation, T.S.; writing—review and editing, T.S., M.I.T. and M.A.; visualization, T.S.; supervision, T.S.; project administration, T.S.; funding acquisition, T.S. All authors have read and agreed to the published version of the manuscript.

Data Availability

The data used to support the research findings are available from the corresponding author upon request.

Conflicts of Interest

The authors declare no conflicts of interest.

References

- [1] A. A. Belal, “Detecting urban growth using remote sensing and GIS techniques in Al Gharbiya governorate, Egypt,” *Egypt. J. Remote Sens. Space Sci.*, vol. 14, pp. 73–79, 2011. <https://doi.org/10.1016/j.ejrs.2011.09.001>
- [2] W. L. Fiho, A. Balogun, O. E. Olayide, U. M. Azeiteiro, D. Y. Ayal, P. D. C. Munoz, G. J. Nagy, P. Bynoe, O. Oguge, N. Y. Toamukum, and et al., “Assessing the impacts of climate change in cities and their adaptive capacity: Towards transformative approaches to climate change adaptation and poverty reduction in urban areas in a set of developing countries,” *Sci. Total Environ.*, vol. 692, pp. 1175–1190, 2019. <https://doi.org/10.1016/j.scitotenv.2019.07.227>
- [3] R. F. M. Ameen and M. Morshed, “Urban environmental challenges in developing countries—A stakeholder perspective,” *Habitat Int.*, vol. 64, pp. 1–10, 2017. <https://doi.org/10.1016/j.habitatint.2017.04.002>
- [4] O. Hamdy, S. Zhao, A. M. Salheen, and Y. Y. Eid, “Identifying the risk areas and urban growth by ArcGIS-tools,” *Geosci.*, vol. 6, no. 4, p. 47, 2016. <https://doi.org/10.3390/geosciences6040047>
- [5] C. Deng and C. Wu, “Examining the impacts of urban biophysical compositions on surface urban heat island: A spectral unmixing and thermal mixing approach,” *Remote Sens. Environ.*, vol. 131, pp. 262–274, 2013. <https://doi.org/10.1016/j.rse.2012.12.020>
- [6] X. Li, Y. Zhou, G. R. Asrar, M. Imhoff, and X. Li, “The surface urban heat island response to urban expansion: A panel analysis for the conterminous United States,” *Sci. Total Environ.*, vol. 605–606, pp. 426–435, 2017. <https://doi.org/10.1016/j.scitotenv.2017.06.229>
- [7] Y. Xiong, S. Huang, F. Chen, H. Ye, C. Wang, and C. Zhu, “The impacts of rapid urbanization on the thermal environment: A remote sensing study of Guangzhou, South China,” *Remote Sens.*, vol. 4, pp. 2033–2056, 2012. <https://doi.org/10.3390/rs4072033>
- [8] D. A. Roberts, P. E. Dennison, K. L. Roth, K. Dudley, and G. Hulley, “Relationships between dominant plant species, fractional cover and land surface temperature in a Mediterranean ecosystem,” *Remote Sens. Environ.*, vol. 167, pp. 152–167, 2015. <https://doi.org/10.1016/j.rse.2015.01.026>
- [9] B. J. He, J. Zhu, D. X. Zhao, Z. H. Gou, J. D. Qi, and J. S. Wang, “Co-benefits approach: Opportunities for implementing sponge city and urban heat island mitigation,” *Land Use Policy*, vol. 86, pp. 147–157, 2019. <https://doi.org/10.1016/j.landusepol.2019.05.003>
- [10] J. Huang, H. Yu, A. Dai, Y. Wei, and L. Kang, “Drylands face potential threat under 2°C global warming target,” *Nat. Clim. Change*, vol. 7, pp. 417–422, 2017. <https://doi.org/10.1038/NCLIMATE3275>
- [11] C. Hong, Q. Zhang, Y. Zhang, S. Davis, D. Tong, Y. Zheng, Z. Liu, D. Guan, K. He, and H. Schellnhuber, “Impacts of climate change on future air quality and human health in China,” *Proc. Natl. Acad. Sci.*, vol. 116, pp. 17 193–17 200, 2019. <https://doi.org/10.1073/pnas.1812881116>
- [12] H. Orru, K. Ebi, and B. Forsberg, “The interplay of climate change and air pollution on health,” *Curr. Environ. Health Rep.*, vol. 4, pp. 504–513, 2017. <https://doi.org/10.1007/s40572-017-0168-6>

- [13] S. Abdul-Nabi, V. Karaki, A. Khalil, and T. Zahran, "Climate change and its environmental and health effects from 2015 to 2022: A scoping review," *Heliyon*, vol. 11, no. 3, p. e42315, 2025. <https://doi.org/10.1016/j.heliyon.2025.e42315>
- [14] United Nations Human Settlements Programme (UN-Habitat), "World Cities Report 2020: The Value of Sustainable Urbanization," 2020. <https://unhabitat.org/world-cities-report-2020-the-value-of-sustainable-urbanization>
- [15] S. Esfandeh, A. Danehkar, A. Salmanmahiny, S. M. M. Sadeghi, and M. V. Marcu, "Climate change risk of urban growth and land use/land cover conversion: An in-depth review of the recent research in Iran," *Sustainability*, vol. 14, no. 1, p. 338, 2021. <https://doi.org/10.3390/su14010338>
- [16] UN DESA, "UN report: Delivering on international commitments is fundamental to meet the MDGs," 2010. <https://www.un.org/en/development/desa/news/policy/un-report-delivering.html>
- [17] S. Chapman, M. Thatcher, A. Salazar, J. E. Watson, and C. A. McAlpine, "The impact of climate change and urban growth on urban climate and heat stress in a subtropical city," *Int. J. Climatol.*, vol. 39, no. 6, pp. 3013–3030, 2019. <https://doi.org/10.1002/joc.5998>
- [18] A. Abulibdeh, S. Pirasteh, D. Mafi-Gholami, M. Kucukvar, N. C. Onat, and E. Zaidan, "Unveiling the nexus between land use, land surface temperature, and carbon footprint: A multi-scale analysis of building energy consumption in arid urban areas," *Earth Syst. Environ.*, vol. 9, pp. 1–39, 2024. <https://doi.org/10.1007/s41748-024-00550-6>
- [19] P. D. Hien, N. T. Men, P. M. Tan, and M. Hangartner, "Impact of urban expansion on the air pollution landscape: A case study of Hanoi, Vietnam," *Sci. Total Environ.*, vol. 702, p. 134635, 2020. <https://doi.org/10.1016/j.scitotenv.2019.134635>
- [20] J. Ji, S. Wang, Y. Zhou, W. Liu, and L. Wang, "Spatiotemporal change and landscape pattern variation of eco-environmental quality in Jing-Jin-Ji urban agglomeration from 2001 to 2015," *IEEE Access*, vol. 8, pp. 125 534–125 548, 2020. <https://doi.org/10.1109/ACCESS.2020.3007786>
- [21] R. M. Aurora and K. Furuya, "Spatiotemporal analysis of urban sprawl and ecological quality study case: Chiba Prefecture, Japan," *Land*, vol. 12, no. 11, 2024. <https://doi.org/10.3390/land12112013>
- [22] P. R. Ranasinghe, "Zoning, land use management and nature-based solutions in urban planning, where Sri Lanka is standing," in *Proceedings of International Forestry and Environment Symposium*, 2024, p. 293. <https://doi.org/10.31357/fesympo.v28.7145>
- [23] M. Maharjan, A. Aryal, B. M. Shakya, R. Talchabhadel, B. R. Thapa, and S. Kumar, "Evaluation of urban heat island (UHI) using satellite images in densely populated cities of South Asia," *Earth*, vol. 2, no. 1, pp. 86–110, 2021. <https://doi.org/10.3390/earth2010006>
- [24] Z. Venter, O. Brousse, I. Esau, and F. Meier, "Hyperlocal mapping of urban air temperature using remote sensing and crowdsourced weather data," *Remote Sens. Environ.*, vol. 242, p. 111791, 2020. <https://doi.org/10.1016/j.rse.2020.111791>
- [25] Y. Yang, C. Cao, X. Pan, X. Li, and X. Zhu, "Downscaling land surface temperature in an arid area by using multiple remote sensing indices with random forest regression," *Remote Sens.*, vol. 9, no. 8, p. 789, 2017. <https://doi.org/10.3390/rs9080789>
- [26] C. M. Souza Jr, Z. Shimbo, M. R. Rosa, L. L. Parente, A. Alencar, B. F. Rudorff, H. Hasenack, M. Matsumoto, L. G. Ferreira, P. W. Souza-Filho, and T. Azevedo, "Reconstructing three decades of land use and land cover changes in Brazilian biomes with Landsat archive and Earth Engine," *Remote Sens.*, vol. 12, no. 17, p. 2735, 2020. <https://doi.org/10.3390/rs12172735>
- [27] M. I. Hossain and J. Islam, "Impact of urbanization on urban heat island intensity in Mymensingh, Bangladesh: A study using Landsat-8 images on Google Earth Engine," in *7th International Conference on Civil Engineering for Sustainable Development (ICCESD 2024)*, Khulna, Bangladesh, 2024.
- [28] V. Gallina, S. Torresan, A. Zabeo, A. Critto, T. Glade, and A. Marcomini, "A multi-risk methodology for the assessment of climate change impacts in coastal zones," *Sustainability*, vol. 12, no. 9, p. 3697, 2020. <https://doi.org/10.3390/su12093697>
- [29] O. Roa, M. Bachmann, R. Mechler, R. Trogrlić, L. Reimann, M. Mazzoleni, J. Aerts, F. Buskop, A. Pirani, and J. Mysiak, "Challenges and opportunities in climate risk assessment: Future directions for assessing complex climate risks," *Environ. Res. Lett.*, vol. 20, no. 5, pp. 1–14, 2025. <https://doi.org/10.1088/1748-9326/adc756>
- [30] Z. Tang, S. Yi, C. Wang, and Y. Xiao, "Incorporating probabilistic approach into local multi-criteria decision analysis for flood susceptibility assessment," *Stoch. Environ. Res. Risk Assess.*, vol. 32, pp. 701–714, 2018. <https://doi.org/10.1007/s00477-017-1431-y>
- [31] B. Ahmed, M. D. Kamruzzaman, X. Zhu, M. S. Rahman, and K. Choi, "Simulating land cover changes and their impacts on land surface temperature in Dhaka, Bangladesh," *Remote Sens.*, vol. 5, no. 11, pp. 5969–5998, 2013. <https://doi.org/10.3390/rs5115969>

- [32] M. M. Rahman, R. Avtar, A. P. Yunus, J. Dou, P. Misra, W. Takeuchi, and T. Agustiono Kurniawan, “Monitoring the effect of spatial growth on land surface temperature in Dhaka,” *Remote Sens.*, vol. 12, no. 7, p. 1191, 2020. <https://doi.org/10.3390/rs12071191>
- [33] T. Zarin and M. Esraz-Ul-Zannat, “Assessing the potential impacts of LULC change on urban air quality in Dhaka City,” *Ecol. Indic.*, vol. 154, p. 110746, 2023. <https://doi.org/10.1016/j.ecolind.2023.110746>
- [34] S. K. Biswas, B. A. Begum, S. A. Tarafdar, and A. Islam, “Characterization of air pollution at urban sites at Dhaka and Rajshahi in Bangladesh,” *Atomic Energy Centre, Dhaka*, 2016. https://www.researchgate.net/profile/Bilkis-Begum-6/publication/237461485_Characterization_of_air_pollution_at_urban_sites_at_Dhaka_and_Rajshahi_in_Bangladesh/links/572eb74708aee022975a625b/Characterization-of-air-pollution-at-urban-sites-at-Dhaka-and-Rajshahi-in-Bangladesh.pdf?origin=scientificContributions
- [35] M. Rahnuma, M. M. H. Chowdhury, T. R. Ferdousi, A. Ahmed, and N. Ahmed, “The land use and land cover relation with air pollutants of Rajshahi City: A remote sensing approach,” in *7th International Conference on Sustainable Built Environment (ICSBE 2016)*, Kandy, Sri Lanka, 2016.
- [36] A. K. S. Aakash and S. N. Puja, “Assessing the impacts of land use and land cover changes on land surface temperature in rapidly urbanizing environments: A case study of Rajshahi City, Bangladesh,” in *7th International Conference on Civil Engineering for Sustainable Development (ICCESD 2024)*, Khulna, Bangladesh, 2024.
- [37] M. M. Rahman, M. S. Islam, and M. H. Sarker, “Towards green and climate-resilient urbanization in Rajshahi City: Urban growth meets climate action in Northern Bangladesh,” *Urban Clim.*, vol. 45, p. 101365, 2023. <https://doi.org/10.1142/S2345748125500010>
- [38] Bangladesh Bureau of Statistics (BBS), “Bangladesh Population and Housing Census 2022,” 2022. https://bbs.portal.gov.bd/sites/default/files/files/bbs.portal.gov.bd/page/b343a8b4_956b_45ca_872f_4cf9b2f1a6e0/2023-09-27-09-50-a3672cdf61961a45347ab8660a3109b6.pdf
- [39] N. Islam, T. Chowdhury, and A. Karim, “Spatiotemporal urban expansion and its impact on land surface temperature in Dhaka metropolitan area: A GIS-based assessment,” *Remote Sens. Lett.*, vol. 12, no. 3, pp. 398–412, 2021.
- [40] S. Ahmed and M. Hasan, “Urban heat island effects and land surface temperature variation in Dhaka, Bangladesh: A remote sensing analysis,” *Environ. Sci. Policy*, vol. 128, pp. 64–76, 2022.
- [41] M. Hossain, A. Rahman, and S. Alam, “Land use and land cover changes in Rajshahi City: Impacts on local climate and environment,” *J. Urban Stud.*, vol. 18, no. 4, pp. 229–244, 2020.
- [42] S. Rahman, M. Alam, and B. Saha, “Land use transformation and urban heat island effect in Rajshahi: A case study using Landsat data,” *Environ. Monit. Assess.*, vol. 193, p. 472, 2021.
- [43] R. Khatun and M. Mahmud, “Analyzing the relationship between urban growth and temperature rise in Rajshahi using remote sensing techniques,” *J. Geospatial Sci.*, vol. 30, no. 2, pp. 147–165, 2023.
- [44] T. Sultana, J. Hossain, and F. Chowdhury, “Impact of land use changes on land surface temperature: A comparative study of Dhaka and Rajshahi cities,” *Climate Res.*, vol. 78, no. 2, pp. 210–225, 2022. <https://doi.org/10.1007/s41748-021-00243-4>
- [45] M. S. A. Khan, “Water management in Dhaka,” *Water Resour. Dev.*, vol. 24, no. 3, pp. 433–448, 2008.
- [46] R. Abrar, S. Sarkar, K. Nishtha, S. Talukdar, Shahfahad, A. Rahman, A. Islam, and A. Mosavi, “Assessing the spatial mapping of heat vulnerability under urban heat island (UHI) effect in the Dhaka metropolitan area,” *Sustainability*, vol. 14, no. 9, p. 4945, 2022. <https://doi.org/10.3390/su14094945>
- [47] M. S. A. Khan, M. M. Rahman, and M. H. Sarker, “Estimating impacts of micro-scale land use/land cover change on urban heat island effect in Rajshahi, Bangladesh,” *Sci. Prog.*, vol. 1, pp. 1–15, 2022.
- [48] M. Marufuzzaman, M. Khanam, and M. Hasan, “Monitoring the land cover change and its impact on the land surface temperature of Rajshahi City, Bangladesh using GIS and remote sensing techniques,” *J. Geogr. Environ. Earth Sci. Int.*, vol. 25, no. 4, pp. 1–19, 2021. <https://doi.org/10.9734/JGEESI/2021/V25I430278>
- [49] G. Chander, B. L. Markham, and D. L. Helder, “Summary of current radiometric calibration coefficients for Landsat MSS, TM, ETM+, and EO-1 ALI sensors,” *Remote Sens. Environ.*, vol. 113, no. 5, pp. 893–903, 2009. <https://doi.org/10.1016/j.rse.2009.01.007>
- [50] B. L. Markham and J. L. Barker, “Landsat MSS and TM post-calibration dynamic ranges, exoatmospheric reflectances and at-satellite temperatures,” *Landsat Tech. Notes*, vol. 1, no. 3, pp. 3–8, 1986.
- [51] J. W. J. Rouse, R. H. Haas, J. A. Schell, and D. W. Deering, “Monitoring vegetation systems in the Great Plains with ERTS,” *NASA*, 1974. <https://ntrs.nasa.gov/citations/19740022614>
- [52] T. N. Carlson and D. A. Ripley, “On the relation between NDVI, fractional vegetation cover, and leaf area index,” *Remote Sens. Environ.*, vol. 62, no. 3, pp. 241–252, 1997. [https://doi.org/10.1016/S0034-4257\(97\)00104-1](https://doi.org/10.1016/S0034-4257(97)00104-1)
- [53] J. A. Sobrino, J. C. Jiménez-Muñoz, and L. Paolini, “Land surface temperature retrieval from Landsat TM 5,” *Remote Sens. Environ.*, vol. 90, no. 4, pp. 434–440, 2004. <https://doi.org/10.1016/j.rse.2004.02.003>

- [54] J. C. Jiménez-Muñoz and J. A. Sobrino, “A generalized single-channel method for retrieving land surface temperature from remote sensing data,” *J. Geophys. Res. Atmos.*, vol. 108, no. 22, p. 4688, 2003. <https://doi.org/10.1029/2003JD003480>
- [55] M. Belgiu and L. Drăguț, “Random forest in remote sensing: A review of applications and future directions,” *ISPRS J. Photogramm. Remote Sens.*, vol. 114, pp. 24–31, 2016. <https://doi.org/10.1016/j.isprsjprs.2016.01.011>
- [56] R. G. Congalton, “A review of assessing the accuracy of classifications of remotely sensed data,” *Remote Sens. Environ.*, vol. 37, no. 1, pp. 35–46, 1991. [https://doi.org/10.1016/0034-4257\(91\)90048-B](https://doi.org/10.1016/0034-4257(91)90048-B)
- [57] S. Boroushaki and J. Malczewski, “Implementing an extension of the analytical hierarchy process using ordered weighted averaging operators with fuzzy quantifiers in ArcGIS,” *Comput. Geosci.*, vol. 34, no. 4, pp. 399–410, 2008. <https://doi.org/10.1016/j.cageo.2007.04.003>
- [58] M. S. Hassan, R. F. L. Gomes, M. A. H. Bhuiyan, and M. T. Rahman, “Land use and the climatic determinants of population exposure to PM_{2.5} in central Bangladesh,” *Pollutants*, vol. 3, no. 3, pp. 381–395, 2023. <https://doi.org/10.3390/pollutants3030026>
- [59] H. Imran, A. Hossain, A. Islam, A. Rahman, M. Bhuiyan, S. Paul, and A. Alam, “Impact of land cover changes on land surface temperature and human thermal comfort in Dhaka City of Bangladesh,” *Earth Syst. Environ.*, vol. 5, pp. 667–693, 2021. <https://doi.org/10.1007/s41748-021-00243-4>
- [60] M. M. Rahman and S. Haque, “Retrieving spatial variation of aerosol level over urban mixed land surfaces using Landsat imageries: Degree of air pollution in Dhaka metropolitan area,” *Phys. Chem. Earth*, vol. 126, p. 103074, 2022. <https://doi.org/10.1016/j.pce.2021.103074>
- [61] Y. Kim and G. Newman, “Climate change preparedness: Comparing future urban growth and flood risk in Amsterdam and Houston,” *Sustainability*, vol. 11, no. 4, p. 1048, 2019. <https://doi.org/10.3390/su11041048>
- [62] Y. Feng, G. Wu, S. Ge, F. Feng, and P. Li, “Identification of key drivers of land surface temperature within the local climate zone framework,” *Land*, vol. 14, no. 4, p. 771, 2025. <https://doi.org/10.3390/land14040771>
- [63] C. M. Souza Jr, Z. Shimbo, M. R. Rosa, L. L. Parente, A. Alencar, B. F. Rudorff, H. Hasenack, M. Matsumoto, L. G. Ferreira, P. W. Souza-Filho, and T. Azevedo, “Reconstructing three decades of land use and land cover changes in Brazilian biomes with Landsat archive and Earth Engine,” *Remote Sens.*, vol. 12, no. 17, p. 2735, 2020. <https://doi.org/10.3390/rs12172735>
- [64] S. E. Gill, J. F. Handley, A. R. Ennos, and S. Pauleit, “Adapting cities for climate change: The role of the green infrastructure,” *Built Environ.*, vol. 33, no. 1, pp. 115–133, 2007. <https://doi.org/10.2148/benv.33.1.115>